Research Square

Preprints are preliminary reports that have not undergone peer review.
They should not be considered conclusive, used to inform clinical practice,
or referenced by the media as validated information.

DMT and harmine responses in monocyte-derived microglia- like cells from patients with treatment-resistant depression

Francisco Cid Coelho Pinto
Federal University of Ceará, Drug Research and Development Center (NPDM)
Fátima Cássia Evangelista Oliveira
Federal University of Ceará, Drug Research and Development Center (NPDM)
Hilda Tahim Souza
Federal University of Ceará, Drug Research and Development Center (NPDM)
José Brito Vieira Neto
Federal University of Ceará, Drug Research and Development Center (NPDM)
Isabelle de Fátima Vieira Camelo Maia
Federal University of Ceará, Drug Research and Development Center (NPDM)
Sérgio André Souza Júnior
Federal University of Ceará, Drug Research and Development Center (NPDM)
Fábio Oliveira Silva Ribeiro
Federal University of the Parnaíba Delta
Alyne Rodrigues Araujo Nobre
Federal University of the Parnaíba Delta
Claudio Costa dos Santos
Federal Rural University of the Semi-Arid Region
Islay Lima Magalhães
Federal University of Ceará, Drug Research and Development Center (NPDM)
Caio Andrade Oliveira
Federal University of Ceará, Drug Research and Development Center (NPDM)
Deysi Viviana Tenazoa Wong
Federal University of Ceará, Drug Research and Development Center (NPDM)
Claudia do Ó Pessoa
Federal University of Ceará, Drug Research and Development Center (NPDM)
David Freitas Lucena
Federal University of Ceará, Drug Research and Development Center (NPDM)
Maria Francilene Souza Silva
Universidade de Fortaleza

Danielle S. Macedo

danielle.macedo@ufc.br

Federal University of Ceará, Drug Research and Development Center (NPDM)

Research Article

Keywords: microglia, monocytes, dimethyltryptamine, harmine, depression, neuroinflammation

Posted Date: November 11th, 2026

DOI: https://doi.org/10.21203/rs.3.rs-11516239/v1

License: This work is licensed under a Creative Commons Attribution 4.0 International License.
Read Full License

Additional Declarations: No competing interests reported.

Abstract

Purpose

To examine cytokine, surface-marker, and morphological responses to N, N-dimethyltryptamine (DMT) and harmine in lipopolysaccharide (LPS)-challenged monocyte-derived microglia-like cells (iMGs) from patients with treatment-resistant depression (TRD).

Methods

This exploratory study used assay-specific subsets of a cohort of four healthy controls and seven patients with TRD. The principal pharmacological assays used TRD-derived iMGs. Parallel cultures were compared under control conditions, LPS alone (100 ng/mL, 24 h), or LPS followed by DMT (90 µg/mL) or harmine (35 µM) for 3 h. Cytokine transcripts and surface-marker positivity were evaluated in four donors, and high-content imaging in three.

Results

DMT increased IL10 expression relative to LPS alone (mean difference, 0.4088; 95% confidence interval, 0.1546–0.6629; Tukey-adjusted p = 0.0134). LPS increased IL6 relative to control (adjusted p = 0.0305), whereas neither compound significantly reduced IL6 after adjustment. CD86 and CD200 positivity showed no significant condition effects. Process number showed an overall condition effect (exact Friedman p = 0.017), without significant drug-versus-LPS contrasts after Holm correction.

Conclusion

IL10 transcription is a candidate response measure for replication. Small donor samples, the absence of matched healthy-control pharmacological assays, and concentration-selection limitations prevent inference about disease specificity, generalized anti-inflammatory activity, or clinical efficacy.

1. Introduction

Microglial cytokine signaling and interactions with other glial cells are implicated in the neurobiology of depression (Haroon et al. 2017; Jia et al. 2021). Recent experiments in a chronic social defeat stress model linked microglial interleukin-6 (IL-6) release to hippocampal astrocyte apoptosis and depression-like behavior (Shen et al. 2025). Microglial states nevertheless depend on context and cannot be reduced to binary resting/activated or M1/M2 categories (Paolicelli et al. 2022). Cytokine, surface-marker, and morphological measurements therefore provide complementary information about cellular responses (Hernangómez et al. 2012; Anderson et al. 2017).

Monocyte-derived microglia-like cells (iMGs) provide an accessible human model for studying donor-associated immune responses (Banerjee et al. 2021; Quek et al. 2022). Their peripheral origin and culture environment distinguish them from resident brain microglia. Treatment-resistant depression (TRD), commonly defined by inadequate response to at least two adequate antidepressant trials, provides a clinically relevant setting for exploratory cellular studies (McIntyre et al. 2023). A recent study profiled iMG transcripts before and after repetitive transcranial magnetic stimulation in five patients with TRD, illustrating the use of this model for hypothesis generation while highlighting the need for larger, controlled studies (Tateishi et al. 2025).

N, N-dimethyltryptamine (DMT) and harmine are pharmacologically distinct constituents of ayahuasca, which showed antidepressant effects in a randomized placebo-controlled TRD trial (Palhano-Fontes et al. 2019). Harmine and related β-carbolines inhibit monoamine oxidase A and increase oral DMT bioavailability (Riba et al. 2012; Berlowitz et al. 2022). More recently, an open-label study of vaporized DMT in TRD and a randomized placebo-controlled trial of intravenous DMT with psychological support in major depressive disorder (MDD) strengthened the rationale for investigating DMT individually (Falchi-Carvalho et al. 2025; Erritzoe et al. 2026). These clinical findings do not establish a microglial mechanism of antidepressant action.

DMT has shown immunomodulatory and cytoprotective effects in human immune and neural cell models, with evidence implicating sigma-1 receptor signaling (Szabo et al. 2014; Szabo et al. 2016). Experimental stroke research also links DMT to blood–brain barrier protection and reduced neuroinflammation (László et al. 2025). Harmine has suppressed NF-κB-associated inflammatory signaling and LPS-related neuroinflammatory responses in preclinical models (Liu et al. 2017; Zheng et al. 2023). These findings motivated assessment of both compounds in patient-derived iMGs; they do not establish their relative efficacy or superiority over other psychedelics. Earlier experiments also linked chronic harmine treatment to antidepressant-like behavior and increased hippocampal brain-derived neurotrophic factor (BDNF) in rats (Fortunato et al. 2010), providing a separate neurobiological rationale for studying this constituent.

We examined cytokine transcripts, surface-marker positivity, and quantitative morphology after DMT or harmine exposure in LPS-challenged TRD-derived iMGs. The parallel-culture, post-challenge design aimed to identify candidate cellular response measures for replication. Additional membrane-integrity and biophysical measurements were exploratory; disease specificity and clinical efficacy were not tested.

2. Materials and methods

2.1 Study design and participants

Healthy controls (HC) and patients with TRD, aged 18–55 years, were recruited from the same catchment area. A psychiatrist defined TRD as MDD without a clinically meaningful response after at

least 12 months of treatment with two antidepressants from different classes at adequate doses. Participants were fluent in Portuguese and provided written informed consent. Clinical characterization included psychiatric evaluation, a sociodemographic questionnaire, and the Montgomery–Åsberg Depression Rating Scale (MADRS).

The clinical cohort comprised four HC and seven TRD participants. HC-derived cells contributed to differentiation, phenotypic characterization, and exploratory panoptic morphology under LPS and drug exposure. The principal pharmacological assays used TRD-derived iMGs because of cell availability; no matched HC-versus-TRD response comparison was performed.

HC04 was excluded from cellular assays after a data-collection error and TRD04 after differentiation failure; both remained in the clinical cohort. Another participant was excluded for TRD ineligibility. Donor participation depended on differentiation success, sample yield, and processing priority (Supplementary Table S1).

Patients were recruited through a clinical ketamine-treatment program, and blood was collected before ketamine initiation. Samples were used for the ex vivo experiments; this study did not evaluate clinical ketamine effects.

2.2 Ethical approval

The study was conducted in accordance with the Declaration of Helsinki and Brazilian National Health Council Resolution No. 466/2012. The study protocol was approved by the Research Ethics Committee of the Federal University of Ceará (CAAE 74556423.8.0000.5054). Written informed consent was obtained from all participants before enrollment.

2.3 Test compounds

Crystalline DMT was isolated from *Mimosa tenuiflora* roots collected in Nova Jaguaribara, Ceará, Brazil (voucher no. 9962, HDELTA herbarium), by cold hexane percolation followed by ethanol percolation of the residual material. Identity was verified by gas chromatography–mass spectrometry (Agilent 5977C GC/MSD coupled to an Agilent 8860 gas chromatograph) against a commercial DMT standard (Cayman Chemical, cat. no. 13959) and the NIST spectral library. Measured purity was 97.33%. The experiments therefore used analytically characterized crystalline material rather than crude extract.

Harmine (HRM) was obtained commercially from Sigma-Aldrich (USA; cat. no. 286044; 98% purity). Harmine was dissolved immediately before use according to the manufacturer's recommendations. Crystalline DMT was dissolved in DMSO immediately before use and subsequently diluted in culture medium to the working concentration. DMT concentrations are reported as the mass of the isolated crystalline preparation per unit volume.

2.4 Concentration selection

Working concentrations were guided by MTT assays in an immortalized mouse astrocyte line (Mosmann 1983; Denizot and Lang 1986) and Alamar Blue assays in peripheral blood mononuclear cells (PBMCs) (O'Brien et al. 2000). Astrocyte exposure lasted 24, 48, or 72 h for DMT and 24 or 48 h for harmine; both iMG drug exposures lasted 3 h. Detailed screening methods and IC_{50} estimates are provided in Supplementary Methods S6 and Supplementary Table S2. Limited primary-cell yield precluded direct iMG concentration–response testing. Screening results do not establish microglia-specific safety; propidium iodide (PI) staining provided an additional descriptive membrane-integrity measure (Supplementary Methods S1).

2.5 Inflammatory activation and pharmacological treatment

Drug-response assays compared control, LPS alone, LPS + DMT, and LPS + HRM in parallel cultures from each donor. In the drug-treated conditions, iMGs were exposed to LPS (100 ng/mL; Sigma-Aldrich, cat. no. L2880) for 24 h, followed by DMT (90 µg/mL) or harmine (7.43 µg/mL, equivalent to 35 µM) for 3 h. Both compounds were evaluated over the same post-challenge interval; preventive administration was not investigated.

The nominal DMT concentration corresponds to approximately 478 µM as free-base equivalents without purity correction. This high in vitro exposure exceeds systemic concentrations reported after human ayahuasca administration (Riba et al. 2012) and was not intended to reproduce human pharmacokinetics.

2.6 PBMC isolation and differentiation into microglia-like cells (iMGs)

PBMCs were isolated from approximately 40–50 mL of blood by Histopaque 1077 density-gradient centrifugation (900 × g, 25 min, brakes off), washed twice with phosphate-buffered saline, and cryopreserved in fetal bovine serum containing 10% DMSO. Average yield was approximately 2–3 × 10^6 cells per sample.

Differentiation into monocyte-derived microglia-like cells (iMGs) followed previously described protocols (Banerjee et al. 2021; Quek et al. 2022; Ohgidani et al. 2014; Sellgren et al. 2017). PBMCs were seeded at 2 × 10^5 cells/cm^2 on Geltrex-coated plates in RPMI 1640 supplemented with 10% fetal bovine serum and 1% antibiotics. After 24 h, non-adherent cells were removed, and the medium was replaced with differentiation medium containing RPMI 1640, GlutaMAX, 1% penicillin–streptomycin, IL-34 (100 ng/mL), and GM-CSF (10 ng/mL). We replaced half of the medium on day 6, followed by a complete medium

replacement on day 9 after washing. Differentiated iMGs were used experimentally between days 10 and 14.

Brightfield images acquired on days 1, 6, 9, 11, 12, and 13 documented differentiation. CD11b, CD45, TMEM119, IBA1, and process-bearing morphology were used to characterize the iMG phenotype, without implying equivalence to resident microglia.

2.6.1 Flow cytometry

Differentiated iMGs were resuspended in 1% bovine serum albumin (BSA) and incubated for 30 min with the indicated antibodies. Flow-cytometry acquisition was performed using an Attune™ NxT Flow Cytometer (Thermo Fisher Scientific) equipped with a blue laser. Cells were stained with FITC-conjugated anti-CD11b (clone M1/70, Thermo Fisher Scientific/Invitrogen eBioscience, cat. no. 11-0112-82), PE-conjugated anti-CD45 (clone 30-F11, Thermo Fisher Scientific/Invitrogen eBioscience, cat. no. 12-0451-82), PE-Cy7-conjugated anti-CD200 (Thermo Fisher Scientific/Invitrogen eBioscience, cat. no. 46-5201-42), Alexa Fluor 488-conjugated anti-TMEM119 (clone V3RT1GOsz, Thermo Fisher Scientific/Invitrogen eBioscience, cat. no. 53-6119-82), and PE-Cyanine7-conjugated anti-CD86 (clone GL1, Thermo Fisher Scientific/Invitrogen eBioscience, cat. no. 25-0862-82).

CD11b/CD45 were assessed by dual staining; CD200 and TMEM119 were evaluated separately. Unstained and single-stained controls supported background assessment, positivity thresholds, and FITC/PE compensation. Forward- and side-scatter gates excluded debris. Acquisition yielded approximately 2,000–10,000 events per sample, depending on cell availability. Floreada.io was used to calculate percentages of positive events within the gated population. High background limited TRD03 CD11b/CD45 interpretation (Supplementary Fig. S1). Further acquisition and gating details are provided in Supplementary Methods S4.

2.6.2 Gene expression by RT-qPCR

RNA was extracted using TRIzol (Invitrogen) immediately after the protocol or after storage at −80°C for up to 1 week. Concentration was measured spectrophotometrically at 260 nm, with 260/280 and 260/230 ratios used as purity indicators.

Complementary DNA (cDNA) was synthesized from 500 ng of total RNA in a 20-µL reaction using the GoScript Reverse Transcription System (Promega) and a Veriti thermal cycler (Applied Biosystems), according to the manufacturer's instructions. The cDNA was subsequently diluted with ultrapure water to 20 ng/µL.

Primers targeting IL10, IL6, TNF, TGFB1, ACTB, and GAPDH were designed using NCBI Primer-BLAST and used at a final concentration of 500 nM (Supplementary Table S3). Amplification efficiency was assessed using standard curves generated from serial cDNA dilutions, with quantification cycle (Cq)

plotted against log-transformed template concentration. Quantitative PCR was performed in 10-µL reactions using GoTaq qPCR Master Mix (Promega) on a CFX Opus 96 Real-Time PCR System (Bio-Rad). Reactions were performed in technical duplicate and included no-template controls for all genes. Melting-curve analysis was performed after amplification to assess product specificity.

ACTB and GAPDH stability was evaluated using RefFinder. Technical duplicate Cq values were averaged, and transcript abundance was calculated as $2^{-\Delta Cq}$, where ΔCq was the target-gene Cq minus the mean ACTB/GAPDH Cq.

2.6.3 Immunofluorescence and high-content imaging

Differentiated iMGs were fixed with 4% paraformaldehyde for 20 min at room temperature, permeabilized, and blocked with 2% bovine serum albumin for 1 h. A microglia-associated phenotype was assessed by overnight incubation at 4°C with a goat polyclonal anti-IBA1 antibody (ionized calcium-binding adaptor molecule 1; Santa Cruz Biotechnology, cat. no. sc-28530), followed by incubation with a donkey anti-goat IgG H&L secondary antibody conjugated to Alexa Fluor 488 (Abcam, cat. no. ab150129).

F-actin was labeled using the CytoPainter F-actin Staining Kit, Red Fluorescence (Abcam, cat. no. ab112127), to visualize the actin cytoskeleton and cellular processes. Nuclei were counterstained with 0.002% DAPI (4',6-diamidino-2-phenylindole) in PBS (Thermo Fisher Scientific) for 30 min. Slides were mounted using ProLong Gold Antifade Mountant (Thermo Fisher Scientific).

High-content imaging (HCI) used an Opera Phenix Plus system (Revvity) with a 40× water-immersion objective (NA 1.1). IBA1, F-actin, and DAPI channels were collected for automated morphological analysis, and representative fields illustrated each condition.

2.6.4 Automated image analysis

For each donor and condition, three optical sections per z-stack were acquired across multiple fields on each of two technical replicate slides (L1 and L2). Maximum-intensity projections were used for image analysis.

Harmony 5.2 software (Revvity) was used with an adapted “RMS Neurite Outgrowth Analysis 2 + Morphology” sequence. DAPI identified nuclei and defined the “All Cells” population; the corresponding fluorescence channels delineated cytoplasm and cell bodies.

The Alexa Fluor 488 channel supported IBA1-based segmentation and process detection, with F-actin as a complementary channel. Processes were detected using CSIRO Neurite Analysis 2 (“Find Neurites”). The “Remove Border Objects” filter excluded truncated cells.

The pipeline generated process and cellular descriptors. Prespecified quantitative outcomes were maximum process width and process number per cell.

HCI included TRD01, TRD02, and TRD03. Slide-level measurements were averaged within donor and condition, yielding three biological replicates. No post-hoc cell, field, slide, or donor outlier exclusions were applied.

2.7 Statistical analysis

The donor was the biological experimental unit in participant-derived assays. Wells, slides, fields, cells, flow-cytometry events, and atomic force microscopy (AFM) regions were technical or nested observations. Available technical replicates were averaged within donor and condition before inference.

Continuous clinical variables are reported as mean ± standard deviation and were compared between healthy controls and patients with TRD using two-sided Mann–Whitney U tests with exhaustive permutation of group labels while retaining tied ranks. Categorical variables were compared using Fisher's exact test.

RT-qPCR analyses used $2^{-\Delta Cq}$ values without further transformation (GraphPad Prism 11.0.2). IL10, TNF, and TGFB1 were analyzed by one-way repeated-measures ANOVA with condition as the within-donor factor. IL6 was analyzed with a mixed-effects model fitted by restricted maximum likelihood (REML), with condition as a fixed within-donor effect and donor as a random effect, because one LPS + HRM observation was missing. Overall tests used Geisser–Greenhouse correction. All six pairwise comparisons per gene used Tukey adjustment. Effects are mean differences on the $2^{-\Delta Cq}$ scale with multiplicity-adjusted 95% confidence intervals where applicable. Each condition included four donors, except IL6 under LPS + HRM (n = 3).

CD86 and CD200 percentages were analyzed as paired donor-level repeated measurements using the Friedman test. Donor-level trajectories were additionally displayed to characterize inter-individual variability.

HCI condition effects were assessed by exact permutation Friedman tests, with Kendall's W as the effect size. Exact two-sided sign-flip tests evaluated three prespecified paired contrasts: LPS + DMT versus LPS, LPS + HRM versus LPS, and LPS + DMT versus LPS + HRM. Holm adjustment was applied across these contrasts.

Panoptic morphology and AFM were descriptive because each involved two donors; PI results were also descriptive. Missing values were not imputed. Two-sided $\alpha = 0.05$ was used. Multiplicity correction was applied within each gene or HCI contrast family, not across all endpoints; inference was therefore exploratory.

2.8 Manuscript preparation

ChatGPT (OpenAI) assisted with language editing, manuscript organization, and consistency checks. It was not used to generate or alter primary experimental data or images. The authors are responsible for verification of the cited sources, scientific interpretation, and the final manuscript.

3. Results

3.1 Cohort, concentration selection, and iMG characterization

The cohort comprised four healthy controls and seven patients with TRD; assay participation varied with differentiation success and cell availability (Supplementary Table S1). Mean MADRS scores were 3.50 ± 1.29 and 40.29 ± 5.15, respectively (exact permutation p = 0.0061). Clinical characteristics and item-level scores are reported in Supplementary Results S4, Supplementary Table S4, and Supplementary Fig. S5.

DMT (90 µg/mL) and harmine (35 µM) were selected below astrocyte and PBMC screening IC_{50} estimates, without establishing absence of iMG toxicity (Supplementary Results S5; Supplementary Tables S2 and S5; Supplementary Fig. S6). PI observations showed no consistent additional treatment-associated increase over LPS alone and remained descriptive (Supplementary Results S1).

Differentiation produced adherent, process-bearing cells and increased $CD11b^{+}CD45^{+}$ proportions, consistent with myeloid enrichment (Supplementary Results S6; Supplementary Fig. S7). These observations do not establish resident microglial identity. TRD03 showed substantial unstained background, limiting interpretation of that donor's CD11b/CD45 percentage (Supplementary Fig. S1).

3.2 Surface-marker responses

3.2.1 TMEM119 positivity

TMEM119 was assessed descriptively in TRD03 only. Positivity was 52.48% in control, 20.84% after LPS, 27.93% after LPS + DMT, and 29.03% after LPS + HRM (Fig. 1A). No treatment-related inference was drawn from this single donor.

3.2.2 CD86 and CD200 positivity

CD86 positivity was high across all experimental conditions in the four-donor subset comprising TRD03, TRD05, TRD06, and TRD07. Mean CD86 positivity was 90.82 ± 4.09% under control conditions, 90.41 ± 4.60% after LPS, 88.88 ± 4.19% after LPS + DMT, and 90.30 ± 5.64% after LPS + harmine. No overall condition effect was detected (Friedman $\chi^2 = 2.85$, $p = 0.416$; Supplementary Table S6; Fig. 1B–C).

A sensitivity analysis including TRD02 yielded the same interpretation (p = 0.306). High baseline positivity suggests a potential ceiling effect; percentage-positive measurements cannot exclude changes in expression intensity per cell.

CD200 positivity was 81.66 ± 10.39% in control, 82.84 ± 11.98% after LPS, 80.52 ± 10.63% after LPS + DMT, and 85.56 ± 8.14% after LPS + HRM (Friedman $\chi^2 = 1.20$, p = 0.753; Fig. 1D–E). Harmine-associated changes differed in direction between donors.

3.3 Cytokine expression by RT-qPCR

Relative IL10 expression differed significantly across experimental conditions in the four evaluated TRD donors (repeated-measures ANOVA with Geisser–Greenhouse correction: F(1.494, 4.482) = 13.70, p = 0.0141; Fig. 2A). DMT increased IL10 expression relative to LPS alone in all four donors, with a mean difference of 0.4088 on the $2^{-\Delta Cq}$ scale (95% CI, 0.1546–0.6629; Tukey-adjusted p = 0.0134). IL10 expression was also higher after LPS + DMT than under control conditions (mean difference, 0.4135; 95% CI, 0.1749–0.6521; adjusted p = 0.0109). In contrast, the LPS + harmine versus LPS comparison was not significant (mean difference, 0.1613; 95% CI, −0.2930 to 0.6155; adjusted p = 0.4478), and the direct DMT-versus-harmine comparison was also not significant (adjusted p = 0.2500).

Relative IL6 expression showed an overall condition effect in the mixed-effects analysis (REML with Geisser–Greenhouse correction: F(1.396, 3.722) = 8.501, p = 0.0442; Fig. 2B). LPS increased IL6 expression relative to control (Tukey-adjusted p = 0.0305). Although IL6 expression was numerically lower after DMT and harmine than after LPS alone, neither comparison was statistically significant after multiplicity adjustment (adjusted p = 0.1583 and 0.2359, respectively). Comparisons involving harmine included three matched donors because one IL6 measurement was unavailable.

No overall condition effect was detected for TNF (F(2.072, 6.215) = 1.779, p = 0.2453; Fig. 2C) or TGFB1 (F(1.382, 4.146) = 2.139, p = 0.2236; Fig. 2D), and none of the corresponding Tukey-adjusted pairwise comparisons was significant. Four donors contributed complete measurements for both genes.

3.4 High-content imaging (HCI) of iMG morphology

HCI included three TRD donors, with technical slides averaged within donor and condition. Representative IBA1 and F-actin images are shown in Fig. 3A–B.

Maximum process width showed no significant condition effect (exact Friedman statistic = 5.80, p = 0.148; Kendall's W = 0.64; Fig. 3C). Although width was numerically greater after harmine than LPS in all donors, this contrast was not significant (exact p = 0.25; Holm-adjusted p = 0.75).

Process number showed an overall condition effect (exact Friedman statistic = 8.20, p = 0.017; Kendall's W = 0.91; Fig. 3D). Neither DMT nor harmine differed significantly from LPS in paired contrasts (exact p = 0.25; Holm-adjusted p = 0.75 for both). These results indicate condition-related variability without establishing a drug-specific morphological effect.

4. Discussion

DMT was associated with increased IL10 transcription in all four TRD donors evaluated by RT-qPCR. This response was not accompanied by statistically supported reductions in IL6 or consistent changes across the other molecular and morphological endpoints. The findings identify a candidate transcriptional response without establishing a coordinated anti-inflammatory program.

4.1 Cytokine and morphological responses to DMT and harmine

Previous studies reported DMT-associated immunomodulation in human monocyte-derived dendritic cells and cytoprotection in neural cell models (Szabo et al. 2014; Szabo et al. 2016). More recent stroke experiments showed DMT-associated changes in vascular integrity and inflammatory readouts, with evidence for sigma-1 receptor involvement (László et al. 2025). These findings support investigating DMT across neuroimmune models but cannot establish the mechanism underlying the present IL10 response. We measured neither receptor engagement nor IL-10 protein; increased transcription cannot be equated with cytokine secretion or anti-inflammatory function.

Neither compound significantly reduced IL6 relative to LPS after correction. This is relevant because recent mouse experiments linked microglial IL-6 to astrocyte injury and depression-like behavior (Shen et al. 2025); our data do not establish modulation of that pathway. Harmine-associated reductions in LPS-related inflammatory responses reported in mice (Zheng et al. 2023) also cannot be assumed in a brief post-challenge human-cell experiment. The nonsignificant direct DMT-versus-harmine comparison does not establish different efficacy between compounds.

Surface-marker percentages captured a different dimension of cellular response. High CD86 positivity may have restricted assay sensitivity, whereas CD200 responses varied among donors. These measurements do not quantify antigen abundance per cell, and the single-donor TMEM119 observations cannot establish restoration of a microglia-associated phenotype.

The HCI condition effect on process number was not accompanied by significant drug-versus-LPS contrasts. With only three paired donors, exact pairwise tests have limited resolution. Moreover, morphology is not a direct surrogate for inflammatory function, consistent with frameworks that define microglial states using complementary molecular and functional evidence (Paolicelli et al. 2022). Panoptic observations from two healthy controls and AFM findings from two TRD donors remain descriptive (Supplementary Results S2–S3; Supplementary Figs. S2–S4).

4.2 Methodological considerations and study limitations

Matched HC pharmacological measurements were unavailable. HC characterization and exploratory panoptic observations cannot establish TRD specificity or normalization toward a healthy phenotype. LPS provided a standardized inflammatory challenge and was not intended to reproduce a TRD-specific immune phenotype.

Small, assay-dependent donor samples limit precision and interpretation of null results. Four donors contributed most RT-qPCR and surface-marker measurements, three contributed HCI, and fewer contributed descriptive assays. Distributional assumptions for the $2^{-\Delta Cq}$ analyses are difficult to assess with four donors. Correction within outcomes rather than across all endpoints limits confirmatory interpretation. Concomitant medication and clinical heterogeneity also constrain attribution to TRD.

Astrocyte and PBMC screens cannot establish suitable human iMG exposures because species and cellular lineage differ. DMT at approximately 478 μM exceeds reported human systemic concentrations (Riba et al. 2012). Descriptive PI findings cannot exclude toxicity or distinguish specific pharmacology from cellular stress. Lower concentrations, direct iMG viability measurements, and concentration–response experiments are needed to establish the relevance of the IL10 signal.

DMT was an analytically characterized crystalline preparation with 97.33% purity. Contributions from residual constituents cannot be excluded. Replication with independently sourced reference-grade DMT would strengthen attribution of the observed response to the compound.

The post-LPS protocol addresses responses after inflammatory challenge and does not test prevention of LPS-induced reactivity. Responses may also depend on the treatment interval, which was limited to 3 h.

Finally, iMGs retain a peripheral monocyte origin and lack the brain cellular environment. Recent TRD iMG transcriptomics supports the feasibility of donor-derived investigations, but does not validate these cells as a proxy for in vivo microglial treatment responses (Tateishi et al. 2025). Blood collection before ketamine initiation avoids conflating the assays with acute ketamine exposure. The DMT clinical trials motivate further research (Falchi-Carvalho et al. 2025; Erritzoe et al. 2026), but the present ex vivo findings neither explain antidepressant effects nor predict clinical outcomes. Recent work reported behavioral and neurochemical effects of ayahuasca in rats exposed to early-life stress (Lodetti et al. 2026). Because ayahuasca contains several active alkaloids, those findings cannot attribute a cellular mechanism to DMT or harmine individually.

4.3 Conclusions and future directions

In this exploratory patient-derived model, DMT was associated with increased IL10 transcription, with limited evidence for broader inflammatory or morphological modulation. Replication should combine larger donor samples, matched healthy-control assays, lower exposure ranges, cytokine protein measurements, and mechanistic experiments.

Declarations

Author contributions

Francisco Cid Coelho Pinto: Conceptualization, Investigation, Methodology, Data curation, Formal analysis, Validation, Visualization, Writing – original draft, Writing – review & editing. Fátima de Cássia Evangelista de Oliveira: Investigation, Methodology, Data curation, Formal analysis, Writing – review & editing. Hilda Tahim de Souza: Investigation, Data curation, Formal analysis, Writing – review & editing. José de Brito Vieira Neto: Methodology, Data curation, Investigation, Formal analysis, Validation, Writing – review & editing. Isabelle de Fátima Vieira Camelo Maia: Methodology, Data curation, Investigation, Formal analysis, Validation, Writing – review & editing. Sérgio André de Souza Júnior: Methodology, Investigation, Resources, Data curation, Writing – review & editing. Adriano José Maia Chaves Filho: Software, Formal analysis, Visualization, Methodology, Investigation, Writing – review & editing. Fábio de Oliveira Silva Ribeiro: Methodology, Data curation, Investigation, Formal analysis, Validation, Writing – review & editing. Alyne Rodrigues de Araujo Nobre: Methodology, Data curation, Formal analysis, Validation, Writing – review & editing. Claudio Costa dos Santos: Methodology, Investigation. Islay Lima Magalhães: Methodology, Investigation. Caio Andrade de Oliveira: Methodology, Investigation. Deysi Viviana Tenazoa Wong: Investigation, Data curation, Writing – review & editing. Claudia do Ó Pessoa: Investigation, Data curation, Writing – review & editing. David Freitas de Lucena: Investigation, Formal analysis, Writing – review & editing. Maria Francilene Souza Silva: Investigation, Methodology, Data curation, Formal analysis, Writing – review & editing. Danielle S. Macedo: Conceptualization, Supervision, Funding acquisition, Project administration, Resources, Writing – review & editing.

Competing interests

The authors declare that they have no known competing financial interests or personal relationships that could have appeared to influence the work reported in this paper.

Data availability

The data supporting the findings of this study are available from the corresponding author upon reasonable request.

Ethics approval and consent to participate

The study was approved by the Research Ethics Committee of the Federal University of Ceará (CAAE 74556423.8.0000.5054). Written informed consent was obtained from all participants.

Supplementary information

Online Resource 1 contains supplementary methods, descriptive results, donor characteristics, screening data, primer sequences, and supporting figures and tables.

References

1. Anderson WD, Greenhalgh AD, Takwale A, David S, Vadigepalli R (2017) Novel influences of IL-10 on CNS inflammation revealed by integrated analyses of cytokine networks and microglial morphology. Front Cell Neurosci 11:233. https://doi.org/10.3389/fncel.2017.00233
2. Banerjee A, Lu Y, Do K, Mize T, Wu X, Chen X et al (2021) Validation of induced microglia-like cells (iMG cells) for future studies of brain diseases. Front Cell Neurosci 15:629279. https://doi.org/10.3389/fncel.2021.629279
3. Berlowitz I, Egger K, Cumming P (2022) Monoamine oxidase inhibition by plant-derived β-carbolines: implications for the psychopharmacology of tobacco and ayahuasca. Front Pharmacol 13:886408. https://doi.org/10.3389/fphar.2022.886408
4. Denizot F, Lang R (1986) Rapid colorimetric assay for cell growth and survival: modifications to the tetrazolium dye procedure giving improved sensitivity and reliability. J Immunol Methods 89:271–277. https://doi.org/10.1016/0022-1759(86)90368-6
5. Erritzoe D, Barba T, Benway T, Joel Z, Good M, Layzell M et al (2026) A short-acting psychedelic intervention for major depressive disorder: a phase IIa randomized placebo-controlled trial. Nat Med 32:591–598. https://doi.org/10.1038/s41591-025-04154-z
6. Falchi-Carvalho M, Palhano-Fontes F, Wießner I, Barros H, Bolcont R, Laborde S et al (2025) Rapid and sustained antidepressant effects of vaporized N,N-dimethyltryptamine: a phase 2a clinical trial in treatment-resistant depression. Neuropsychopharmacology 50:895–903. https://doi.org/10.1038/s41386-025-02091-6
7. Fortunato JJ, Réus GZ, Kirsch TR, Stringari RB, Fries GR, Kapczinski F et al (2010) Chronic administration of harmine elicits antidepressant-like effects and increases BDNF levels in rat hippocampus. J Neural Transm 117:1131–1137. https://doi.org/10.1007/s00702-010-0451-2
8. Haroon E, Miller AH, Sanacora G (2017) Inflammation, glutamate, and glia: a trio of trouble in mood disorders. Neuropsychopharmacology 42:193–215. https://doi.org/10.1038/npp.2016.199
9. Hernangómez M, Mestre L, Correa FG, Loría F, Mecha M, Iñigo PM et al (2012) CD200–CD200R1 interaction contributes to neuroprotective effects of anandamide on experimentally induced inflammation. Glia 60:1437–1450. https://doi.org/10.1002/glia.22366
10. Jia X, Gao Z, Hu H (2021) Microglia in depression: current perspectives. Sci China Life Sci 64:911–925. https://doi.org/10.1007/s11427-020-1815-6
11. László MJ, Vigh JP, Kocsis AE, Porkoláb G, Hoyk Z, Polgár T et al (2025) N,N-dimethyltryptamine mitigates experimental stroke by stabilizing the blood-brain barrier and reducing neuroinflammation. Sci Adv 11:eadx5958. https://doi.org/10.1126/sciadv.adx5958
12. Liu X, Li M, Tan S, Wang C, Fan S, Huang C (2017) Harmine is an inflammatory inhibitor through the suppression of NF-κB signaling. Biochem Biophys Res Commun 489:332–338. https://doi.org/10.1016/j.bbrc.2017.05.126
13. Lodetti G, Redivo H, Teixeira AG, de Farias ACS, de Oliveira Paccagnan L, Rohling JPV et al (2026) Single ayahuasca administration mitigates long-term behavioral and neurochemical effects of early-life stress in rats. J Neural Transm. https://doi.org/10.1007/s00702-026-03287-w

14. McIntyre RS, Alsuwaidan M, Baune BT, Berk M, Demyttenaere K, Goldberg JF et al (2023) Treatment-resistant depression: definition, prevalence, detection, management, and investigational interventions. World Psychiatry 22:394–412. https://doi.org/10.1002/wps.21120
15. Mosmann T (1983) Rapid colorimetric assay for cellular growth and survival: application to proliferation and cytotoxicity assays. J Immunol Methods 65:55–63. https://doi.org/10.1016/0022-1759(83)90303-4
16. O'Brien J, Wilson I, Orton T, Pognan F (2000) Investigation of the Alamar Blue (resazurin) fluorescent dye for the assessment of mammalian cell cytotoxicity. Eur J Biochem 267:5421–5426. https://doi.org/10.1046/j.1432-1327.2000.01606.x
17. Ohgidani M, Kato TA, Setoyama D, Sagata N, Hashimoto R, Shigenobu K et al (2014) Direct induction of ramified microglia-like cells from human monocytes: dynamic microglial dysfunction in Nasu-Hakola disease. Sci Rep 4:4957. https://doi.org/10.1038/srep04957
18. Palhano-Fontes F, Barreto D, Onias H, Andrade KC, Novaes MM, Pessoa JA et al (2019) Rapid antidepressant effects of the psychedelic ayahuasca in treatment-resistant depression: a randomized placebo-controlled trial. Psychol Med 49:655–663. https://doi.org/10.1017/S0033291718001356
19. Paolicelli RC, Sierra A, Stevens B, Tremblay M-E, Aguzzi A, Ajami B et al (2022) Microglia states and nomenclature: a field at its crossroads. Neuron 110:3458–3483. https://doi.org/10.1016/j.neuron.2022.10.020
20. Quek H, Cuní-López C, Stewart R, Lim YC, Roberts TL, White AR (2022) A robust approach to differentiate human monocyte-derived microglia from peripheral blood mononuclear cells. STAR Protoc 3:101747. https://doi.org/10.1016/j.xpro.2022.101747
21. Riba J, McIlhenny EH, Valle M, Bouso JC, Barker SA (2012) Metabolism and disposition of N,N-dimethyltryptamine and harmala alkaloids after oral administration of ayahuasca. Drug Test Anal 4:610–616. https://doi.org/10.1002/dta.1344
22. Sellgren CM, Sheridan SD, Gracias J, Xuan D, Fu T, Perlis RH (2017) Patient-specific models of microglia-mediated engulfment of synapses and neural progenitors. Mol Psychiatry 22:170–177. https://doi.org/10.1038/mp.2016.220
23. Shen S-Y, Liang L-F, Shi T-L, Shen Z-Q, Yin S-Y, Zhang J-R et al (2025) Microglia-derived interleukin-6 triggers astrocyte apoptosis in the hippocampus and mediates depression-like behavior. Adv Sci 12:2412556. https://doi.org/10.1002/advs.202412556
24. Szabo A, Kovacs A, Frecska E, Rajnavolgyi E (2014) Psychedelic N,N-dimethyltryptamine and 5-methoxy-N,N-dimethyltryptamine modulate innate and adaptive inflammatory responses through the sigma-1 receptor of human monocyte-derived dendritic cells. PLoS ONE 9:e106533. https://doi.org/10.1371/journal.pone.0106533
25. Szabo A, Kovacs A, Riba J, Djurovic S, Rajnavolgyi E, Frecska E (2016) The endogenous hallucinogen and trace amine N,N-dimethyltryptamine (DMT) displays potent protective effects against hypoxia

via sigma-1 receptor activation in human primary iPSC-derived cortical neurons and microglia-like immune cells. Front Neurosci 10:423. https://doi.org/10.3389/fnins.2016.00423

26. Tateishi H, Kunitake H, Ohgidani M, Inamine S, Kunitake Y, Murakawa T et al (2025) Does rTMS modulate phenotype of microglia in patients with treatment-resistant depression? A transcriptome analysis using iMG cells. J Affect Disord Rep 21:100919. https://doi.org/10.1016/j.jadr.2025.100919
27. Zheng Z-H, Lin X-C, Lu Y, Cao S-R, Liu X-K, Lin D et al (2023) Harmine exerts anxiolytic effects by regulating neuroinflammation and neuronal plasticity in the basolateral amygdala. Int Immunopharmacol 119:110208. https://doi.org/10.1016/j.intimp.2023.110208

Figures

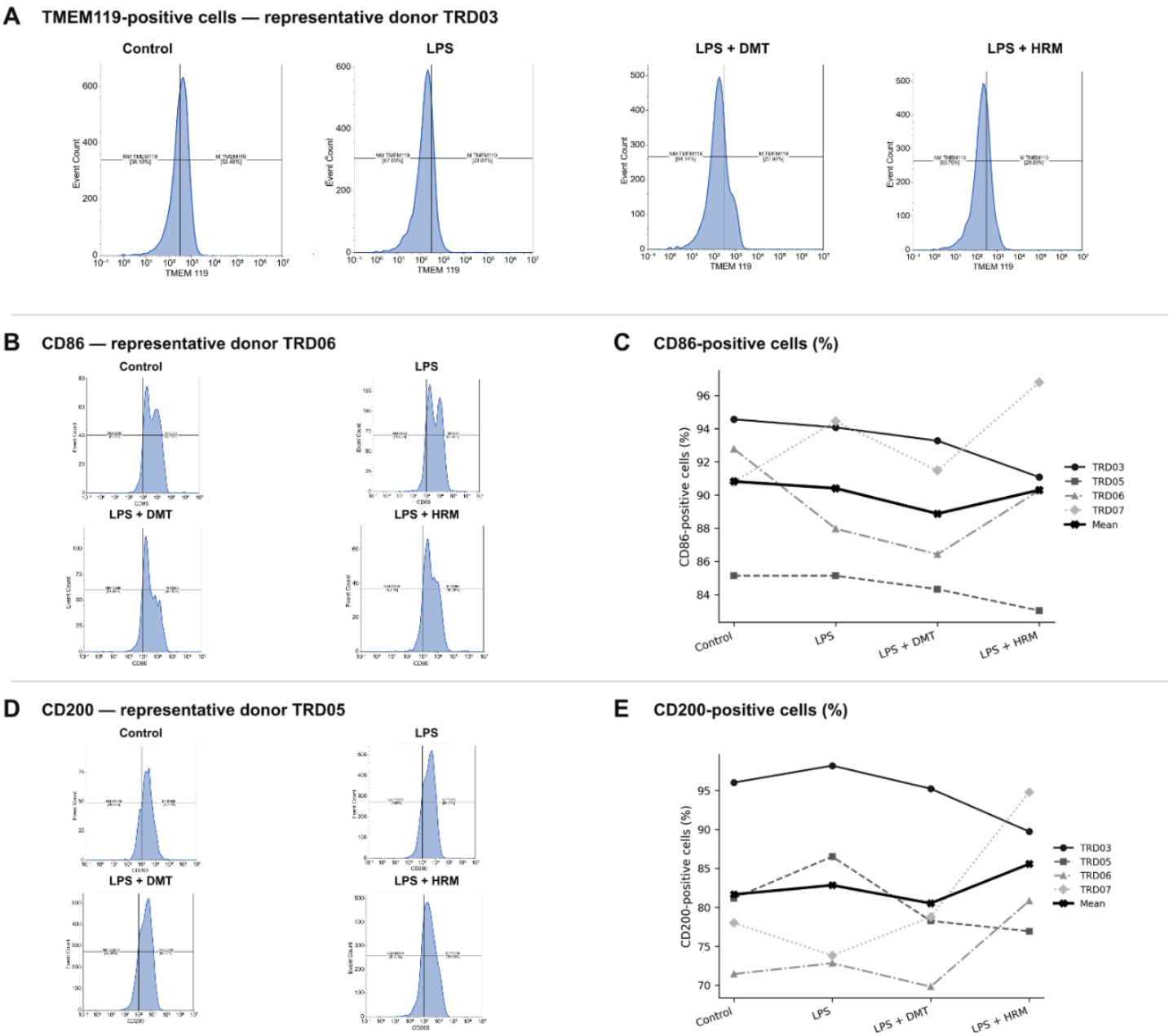


Figure 1

Flow-cytometry analysis of TMEM119, CD86, and CD200 positivity in iMGs. Representative fluorescence distributions are shown for (A) TMEM119 in TRD03, (B) CD86 in TRD06, and (D) CD200 in TRD05 under control, LPS, LPS + DMT, and LPS + HRM conditions. (C, E) Donor-level CD86 and CD200 percentages for TRD03, TRD05, TRD06, and TRD07. Lines connect measurements from each donor; the thicker black line is the mean. TMEM119 is descriptive (n = 1). Friedman tests detected no significant condition effect for CD86 ($\chi^2 = 2.85$, $p = 0.416$) or CD200 ($\chi^2 = 1.20$, $p = 0.753$). High CD86 positivity suggests a possible ceiling effect. DMT, N,N-dimethyltryptamine; HRM, harmine; LPS, lipopolysaccharide

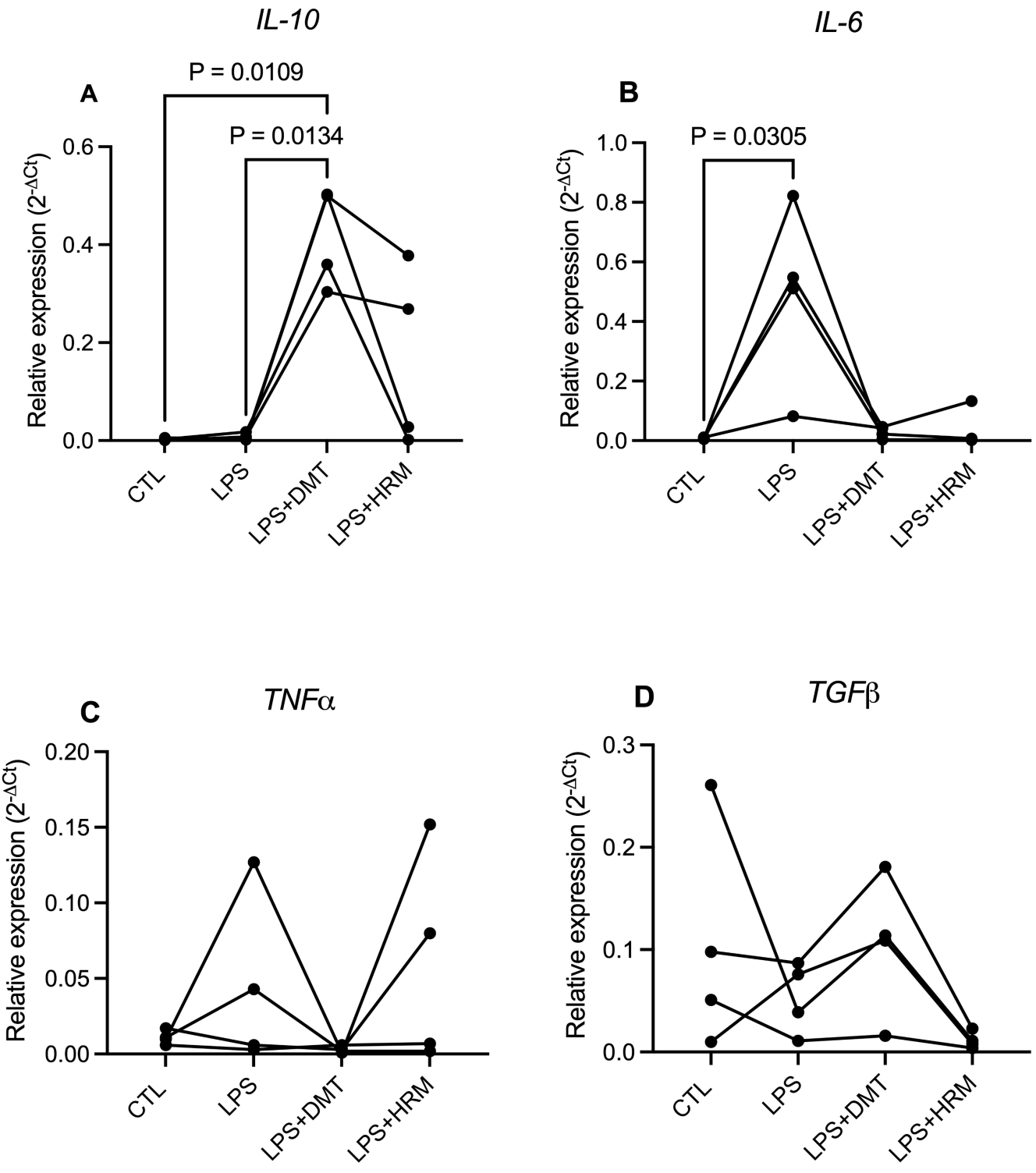


Figure 2

Relative cytokine-gene expression in LPS-challenged patient-derived iMGs. (A) IL10, (B) IL6, (C) TNF (labeled TNFα), and (D) TGFB1 (labeled TGFβ) are displayed as $2^{-\Delta Cq}$ on a linear scale; Ct in the figure denotes Cq. Each line identifies a donor and connects measurements from separate cultures evaluated in parallel under the indicated conditions. The lines represent within-donor pairing and do not indicate a treatment sequence. Each condition includes four donors, except IL6 under LPS + HRM (n = 3); missing values were not imputed. Repeated-measures ANOVA was used for IL10, TNF, and TGFB1, and a REML mixed-effects model for IL6. Analyses used $2^{-\Delta Cq}$ without further transformation, Geisser–Greenhouse correction for overall tests, and Tukey adjustment for all six pairwise comparisons per gene. Displayed adjusted p values are 0.0109 (IL10 control versus LPS + DMT), 0.0134 (IL10 LPS versus LPS + DMT), and 0.0305 (IL6 control versus LPS). Neither DMT nor HRM significantly reduced IL6 relative to LPS (adjusted p = 0.1583 and 0.2359). TNF and TGFB1 showed no significant overall effects. DMT, N,N-dimethyltryptamine; HRM, harmine; LPS, lipopolysaccharide

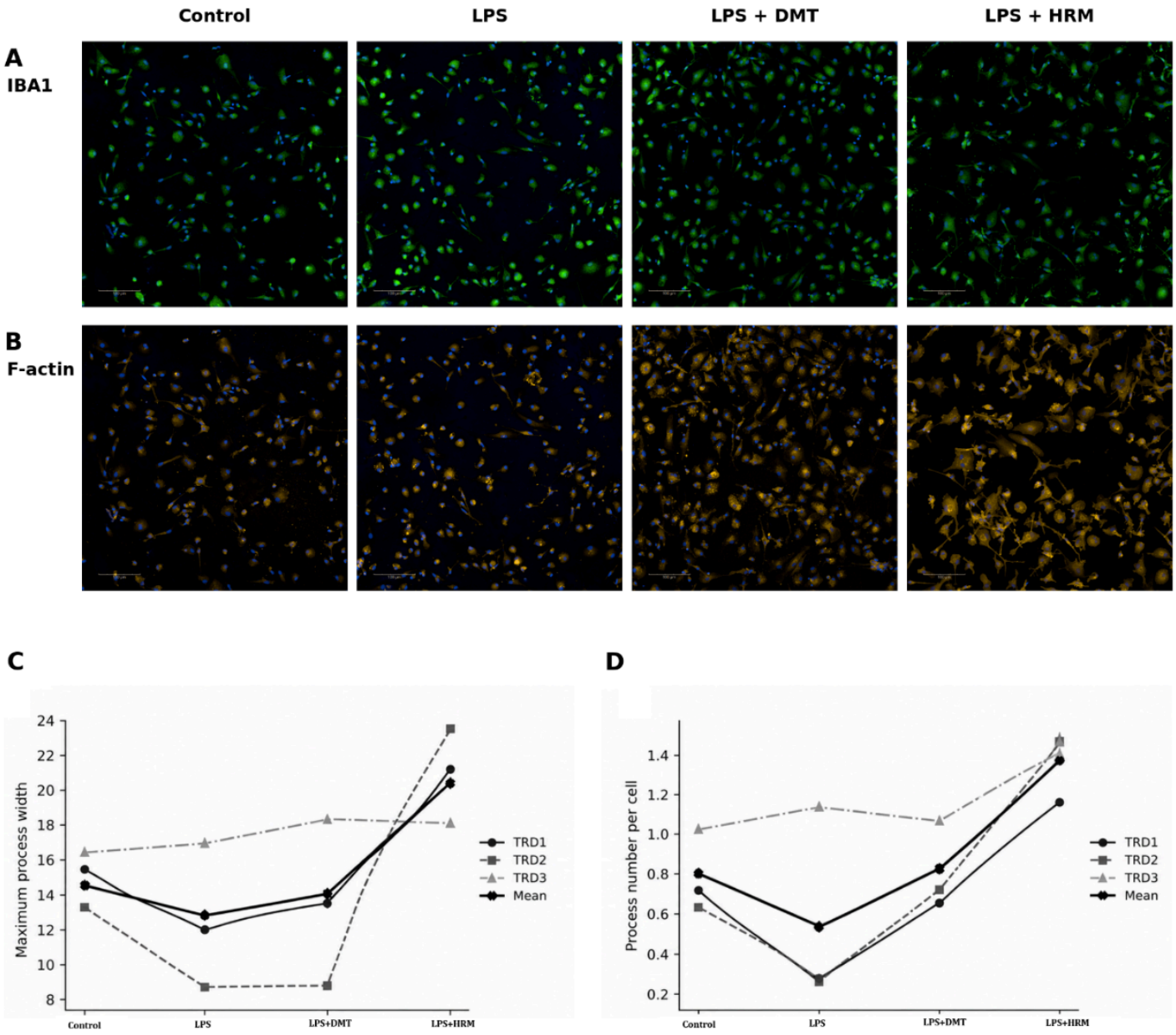


Figure 3

Donor-level high-content imaging analysis of iMG morphology. Representative images showing (A) IBA1 (green) and (B) F-actin (pseudocolored yellow), with DAPI-positive nuclei in blue. (C) Maximum process width and (D) process number per cell in TRD01, TRD02, and TRD03, labeled TRD1, TRD2, and TRD3. Slides L1 and L2 were averaged within donor and condition (n = 3); no post-hoc outlier exclusions were applied. Lines connect donor measurements; the thicker black line is the mean. Exact Friedman tests yielded statistic = 5.80, p = 0.148, and Kendall's W = 0.64 for width, and statistic = 8.20, p = 0.017, and W = 0.91 for process number. Exact two-sided sign-flip tests evaluated three prespecified contrasts: DMT versus LPS, HRM versus LPS, and DMT versus HRM, with Holm adjustment. For process number, neither

drug-versus-LPS contrast was significant (exact p = 0.25; adjusted p = 0.75 for both). All drug conditions followed LPS challenge. DMT, N,N-dimethyltryptamine; HRM, harmine; LPS, lipopolysaccharide

Supplementary Files

This is a list of supplementary files associated with this preprint. Click to download.

- 1.SupplementJNT.pdf